Check for updates

Tinospora cordifolia derived biomass functionalized ZnO particles for effective removal of lead(II), iron(III), phosphate and arsenic(III) from water†

Gaurav Vyas,[ab] Shreya Bhatt [ID] [ab] and Parimal Paul [ID] *[ab]

Owing to the vast diversity in functional groups and cost effectiveness, biomass can be used for various applications. In the present study, biomass from *Tinospora cordifolia* (*TnC*) was prepared and grafted onto the surface of ZnO particles following a simple method. The *TnC* functionalized ZnO particles (ZnO@*TnC*) were characterized and exhibited excellent adsorption properties towards Pb^{2+} (506 mg g^{-1}), Fe^{3+} (358 mg g^{-1}) and PO_4^{3-} (1606 mg g^{-1}) and the Fe^{3+} adsorbed ZnO@*TnC* adsorbs AsO_2^{1-} (189 mg g^{-1}); the metal ions and anions were analyzed by ICP and IC. For reuse of ZnO@*TnC*, a desorption study was successfully carried out using NaOH and EDTA for PO_4^{3-} and Pb^{2+}, respectively; Fe^{3+} was further used for adsorption of As(III). The adsorption fits well with the Langmuir adsorption isotherm model and the adsorption kinetic data are best fitted with a pseudo-second-order equation. The system developed may be useful for treatment of waste water and industrial effluents.

1. Introduction

The unavailability of safe drinking water is one of the major threats to all living species due to the globally polluted environment.[1,2] Toxic heavy metal ion and anion disposal through industrial, mining and agriculture processes is the major reason for the increasing pollution in air, soil and water.[3,4] Heavy metal ions such as Pb^{2+}, Hg^{2+} and AsO_2^{1-} are highly toxic to humans and many other living species even at a very low concentration.[5–7] Lead-acid batteries are highly used for various purposes including in motor vehicles and a recent study suggested that 82% of the global lead consumption is due to lead batteries, which is a major source of lead pollution in the environment.[8,9] Consumption of Pb^{2+} can damage kidneys and severely affect the neurological system.[10,11] Arsenic is another highly toxic ion, the anthropogenic source of its pollution is the metal smelting and coal combustion.[12] Other reasons for arsenic pollution are wood preservation, waste incineration and volcanic emission.[13] Its consumption by human being causes heart disease and cancer of lung, liver, skin and kidney.[14] Iron is an essential metal ion for human body, however above a certain concentration it becomes harmful. It catalyzes formation of reactive oxygen species (ROS), which used to damage nucleic acid and lipid causing Huntington's and Parkinson's diseases.[15] Iron contamination in water is mainly due to its presence in earth crust and other than this natural source, industries of mining and steel are significantly contributing to iron contamination in environment.[4,16] In human body, many intracellular pathways use phosphate ion for important cellular reactions, therefore, control of phosphate is one of the most critical biological regulations. Improper phosphate balance can affect the functionality of almost every human system and can cause kidney disorder, bone problems, weakness and fatigue.[17] Phosphate is key ingredient in fertilizers and above significant concentration can cause algal growth which have significant health and economic hazards. One main example is *Microcystis* algae, which produces microcystin that is lethal to both human as well as aquatic life.[18]

For removal of the above mentioned metal ions and anions, different techniques used are reverse osmosis, ion exchange, solvent extraction, electrochemical methods *etc.*[19–22] ZnO is a biocompatible material and because of its unique physical and chemical properties, it has been used for multifunctional purposes. In the area of separation science, it has been used as an adsorbent for removal of hazardous compound such as H_2S,[23] heavy metal ions *etc.*[24] ZnO particles are available with various size and shape, its surface can also be modified with different coating agent to make it functional material and it has been used for removal of metal ions such as Cu^{2+}, Pb^{2+} *etc.*[25,26] By proper choice of surface modifying agents, the performance of ZnO can be enhanced in terms of adsorption capacity and selectivity towards specific ions/molecules.

[a]Analytical and Environmental Science Division & Centralized Instrument Facility, CSIR-Central Salt and Marine Chemicals Research Institute, G. B. Marg, Bhavnagar 364002, India. E-mail: ppaul@csmcri.res.in

[b]Academy of Scientific and Innovative Research (AcSIR), Ghaziabad-201002, India

With the aim to develop cost effective materials for removal of toxic metal ions and anions from waste/polluted water for its possible recycle, ZnO particles were prepared and the surface of the particles were decorated with the biomass of *Tinospora cordifolia* (ZnO@*TnC*). *Tinospora cordifolia* (*TnC*) is a shrub from the Menispermaceae family, mainly available in the tropical areas, it contains various alkaloids, terpenoids and phenolic compounds having functional groups such as hydroxyl (–OH), carbonyl (–C=O) *etc.*, which can effectively interact with metal ions.[27] This functional material (ZnO@*TnC*) exhibited high adsorption capacity towards the metal ions such as Pb^{2+}, Fe^{3+}, AsO_2^{1-} and anion like PO_4^{3-} in aqueous media. This material can be reused for several time in the case of lead and phosphate, while in the case of iron, it was reused for adsorption of arsenic from waste water. Herein we report preparation of ZnO based biomass decorated functional material, its characterization, metal ion adsorption property and its reusability.

2. Material and methods

2.1. Materials

$Zn(NO_3)_2 \cdot 6H_2O$ was purchased from Alfa Aesar Chemical Company. $NH_2-NH_2 \cdot H_2O$ was purchased from TCI chemical company. Lead chloride ($PbCl_2$), potassium phosphate monobasic (KH_2PO_4), sodium(*meta*)arsenite ($AsNaO_2$), iron chloride ($FeCl_3$) were purchased from Sigma Aldrich. *Tinospora cordifolia* (*TnC*) was collected from Bhavnagar (GPS location: lat. – 21.746746 and long. – 72.14018), Gujarat, India. Synthesis and other study was carried out in double distilled water. All chemicals were used without any further purification.

2.2. Instrumentation

Powder XRD was recorded on a PANalytical Empyrean (PIXcel 3D detector) instrument using Cu Kα ($\lambda = 0.15406$ nm) radiation, operated at 40 kV in the 2θ range of 5° to 80°. FT-IR spectra were recorded on a PerkinElmer instrument, model Spectrum GX, as KBr pellet. Scanning Electron Microscopy (SEM) images were recorded on a JEOL, model JSM 7100F FE-SEM instrument. EDX data was recorded on the Oxford Instrument X-Max^n model. Metal ion analysis was carried out on an ICP-OES instrument from PerkinElmer, model Optima 2000. Ion chromatographic analysis was carried out on a Dionex ICS-5000 + DC model of Thermo Fischer for anions.

2.3. Synthesis of $Zn(OH)_2$ particles

$Zn(NO_3)_2 \cdot 6H_2O$ (2.3 g, 20 mM) was dissolved in 400 mL of double distilled water. In another 400 mL of water, hydrazine hydrate (1.5 mL, 80 mM) was dissolved. Solution of hydrazine hydrate was then added into the solution of $Zn(NO_3)_2 \cdot 6H_2O$ and the reaction mixture was stirred for 4 h at room temperature. The solution was clear at the beginning; however, formation of white precipitates was observed after 10–15 minutes. Solution was allowed to settle for 1 h after completion of stirring for 4 h and then the clear water from the top was decanted. The remaining solution with solid was then centrifuged at 8000 rpm for 15 minutes. The white precipitate thus separated was

isolated, washed with double distilled water (100 mL) for 3 times to remove any excess or unreacted reactants. It was then allowed to dry under vacuum for overnight. The white compound ($Zn(OH)_2$) was characterized by Powder-XRD analysis.

2.4. Preparation of *Tinospora cordifolia* (*TnC*) powder

Leaves and skin of *TnC* were removed manually. Then it was chopped into small pieces and dried at 65 °C for 6 hours. The dried material was crushed by mortar and pestle. The resultant powder was then washed with 0.1 N HCL (100 mL) to remove any existing metal ion and impurities. After acid wash, powder was washed with plenty of water. The powder was characterized by IR and Powder-XRD analysis and was further used for surface modification of ZnO particles.

2.5. Preparation of ZnO@*TnC* particles

TnC powder (4 g) and $Zn(OH)_2$ (1 g), prepared as described above, are mixed well in a crucible and the reaction mixture was heated at 400 °C for 4 h in a muffle furnace. $Zn(OH)_2$ particles at high temperature was converted to ZnO particles due to calcination. After completion of heating, the dark gray colored crystalline mass was obtained, which was then allowed to cool to room temperature, which yielded microcrystals of ZnO@*TnC*. The compound was then characterized on the basis of IR, Powder-XRD and SEM analysis and was used for removal of metal ions.

2.6. Adsorption study with metal ions and anions

Adsorption of various metal ions such as Li^+, Na^+, K^+, Ca^{2+}, Mg^{2+}, Mn^{2+}, Fe^{3+}, Co^{2+}, Ni^{2+}, Cu^{2+}, Hg^{2+}, Pb^{2+}, Cd^{2+} and anions such as AsO_2^{1-}, $Cr_2O_7^{2-}$, CN^-, F^-, PO_4^{3-} were investigated using ZnO@*TnC* material. For this purpose, stock solutions of 10 ppm concentration of each metal ion from its respective chloride salt and of each anion from its respective sodium salt were prepared in 100 mL volumetric flask. In a typical experimental procedure, 10 mg of ZnO@*TnC* was stirred with 100 mL of stock solution of each metal ion and anion at 750 rpm for 6 h. Concentration of metal ions and anions were investigated in samples collected before and after adsorption by inductively coupled plasma (ICP) and ion chromatography (IC).

2.7. Metal ion removal study

The metal ion removal study was carried out at room temperature and at normal pH of Mili-Q water (6.8 ± 0.2) unless otherwise stated. Stock solution of 10, 50 and 100 ppm concentration of Pb^{2+}, PO_4^{3-} and Fe^{3+} was prepared by dissolving required amount of $PbCl_2$, KH_2PO_4 and $FeCl_3$ in double distilled water, respectively. In a typical experiment, 10 mg of ZnO@*TnC* was dispersed into 50 mL of individual stock solution of metal ions and anions of 10, 50 and 100 ppm concentration with stirring at 750 rpm for 6 h. Aqueous samples of 500 μL were collected at regular time interval of 60 minutes by micro pipette and metal ion and anion concentration in the samples were analyzed by ICP and IC, respectively. The ion adsorption

capacity of ZnO@TnC was then calculated using the following eqn (1).[28]

$$q_e = (C_0 - C_e)\frac{V}{m} \qquad (1)$$

where q_e = quantity of metal ion/anion adsorbed on the adsorbent at the time of equilibrium (mg g^{-1}), C_0 = initial concentration of metal ion/anions in aqueous solution (mg L^{-1}), C_e = final concentration of metal ion/anion in aqueous solution at the time t, (mg L^{-1}), V = volume of the solution (L) and m = mass of adsorbents (g).

2.8. pH effect study

Adsorption of metal ions and anions by ZnO@TnC was studied at different pH in the range of 2 to 12. The solutions of that pH range were prepared by adjusting the pH using HCl and NaOH in double distilled water. Stock solution of Pb^{2+}, PO$_4^{3-}$ and Fe^{3+} were prepared of 100 ppm concentration at different pH. In a typical procedure, ZnO@TnC (10 mg) was treated with 50 mL of the stock solution of metal ions and anion with stirring at 750 rpm for 6 h. Aqueous samples (10 mL) were collected from the solutions after 6 h of stirring and analyzed by ICP and IC, as described above.

2.9. Competitive adsorption study

Adsorption capacity of ZnO@TnC towards Pb^{2+}, PO$_4^{3-}$ and Fe^{3+} in the same solution was also studied. A single stock solution containing all of these metal ions and anion was prepared with 100 ppm concentration of each ion in double distilled water. This stock solution (50 mL) containing mixture of ions was treated with 50 mg of ZnO@TnC following the procedure described in the Section 2.8. From the reaction mixture, 10 mL of sample was collected after 6 h of stirring and analyzed by ICP and IC, following the method described above.

2.10. Reusability of ZnO@TnC

Possible recycling of ZnO@TnC was examined by desorption experiment for ions adsorbed into ZnO@TnC. Stock solutions of Pb^{2+}, PO$_4^{3-}$ and Fe^{3+} were prepared of 500 ppm concentration in double distilled water. Then 20 mg of ZnO@TnC for each metal ion and was added into the stock solution (20 mL) of Pb^{2+}, PO$_4^{3-}$ and Fe^{3+} separately, stirred for 6 h (750 rpm) in a conical flask, and then centrifuged at 8000 rpm for 15 minutes. Supernatant liquid was analyzed by ICP and IC to determine the amount of metal ions and anion not adsorbed and ZnO@TnC particles with adsorbed ions were collected and dried in vacuum for overnight. Desorption of PO$_4^{3-}$ from ZnO@TnC material was carried out with the aid of NaOH. The dried ZnO@TnC containing PO$_4^{3-}$ was stirred with 50 mL of 1.0 mol L^{-1} NaOH solution for 1 h at 750 rpm. The resulting solution after stirring was centrifuged for 15 minutes at 8000 rpm and supernatant was collected and analyzed with ion chromatography (IC). The solid ZnO@TnC mass settled after centrifuge was then treated with 0.1 N HCl, washed with water (50 mL) and then reused for the adsorption of phosphate (PO$_4^{3-}$). In case of Pb^{2+}, desorption experiment was carried out with the aid of EDTA. Pb^{2+} adsorbed

ZnO@TnC particles were dispersed in 50 mL of 1.0 mol L^{-1} EDTA solution and stirred for 1 h at 750 rpm. The resultant solution was then centrifuged for 10 minutes at 8000 rpm and supernatant was analyzed by ICP for Pb^{2+}. The settled ZnO@TnC particles were then washed with water (50 mL) and reused for the adsorption of Pb^{2+} in aqueous media. Desorption of iron (Fe^{3+}) from the iron adsorbed ZnO@TnC particles was not successful, however the same was further used for the adsorption of AsO$_2^{1-}$ in aqueous media.

2.11. Synthesis of Fe–ZnO@TnC and its use for removal of AsO$_2^{1-}$

Fe^{3+} adsorbed ZnO@TnC particles were synthesized by stirring 100 mg of ZnO@TnC with 1000 ppm solution of Fe^{3+} at 750 rpm for 6 h followed by centrifugation at 7000 rpm for 10 minutes, the separated particles were then dried for overnight in vacuum. The Fe^{3+} adsorbed ZnO@TnC (Fe–ZnO@TnC) particles (10 mg) were then dispersed into solutions (50 mL) containing AsO$_2^{1-}$ of 10, 50 and 100 ppm and stirred at 750 rpm for 6 h. An aliquot of 500 μL from the solution was collected by micro pipette at a regular interval of 1 h and was analyzed by ion chromatography (IC) to determine the concentration of AsO$_2^{1-}$ in the solution and thereby amount of AsO$_2^{1-}$ adsorbed till the maximum adsorption was achieved. The eqn (1), as written above, was then used to calculate AsO$_2^{1-}$ adsorption capacity of Fe–ZnO@TnC material.

2.12. AsO$_2^{1-}$ adsorption at different pH

Adsorption of AsO$_2^{1-}$ by Fe–ZnO@TnC was studied at different pH in the range 2 to 12. Solutions of AsO$_2^{1-}$ of 100 ppm was prepared with different pH in the range 2 to 12. The solution of AsO$_2^{1-}$ (50 mL) of a particular pH was stirred with Fe–ZnO@TnC (10 mg) at 750 rpm for 6 h, then 10 mL of the solution was taken and analyzed for AsO$_2^{1-}$ by ion chromatography (IC).

2.13. Adsorption isotherm study

Langmuir and Freundlich adsorption isotherm of ZnO@TnC and Fe–ZnO@TnC were studied. For this purpose, solutions of Pb^{2+}, Fe^{3+}, AsO$_2^{1-}$ and PO$_4^{3-}$ of concentration ranging from 10 to 100 ppm were prepared from the respective salts in double distilled water. ZnO@TnC and Fe–ZnO@TnC of 10 mg each were added into the solution of metal ion (50 mL) separately and was stirred for 6 h at 750 rpm. A sample of 10 mL was then collected from the mixture and analyzed for the metal ion/anion by ICP/IC to calculate adsorbed amount of metal ion/anion. The results obtained were then fitted in the equation of Langmuir and Freundlich adsorption isotherm.

3. Results and discussion

3.1. Preparation and characterization of ZnO@TnC particles

The preparation of ZnO@TnC is described in the Experimental section and a schematic presentation is shown in Scheme 1.

In the calcination process at 400 °C, Zn(OH)$_2$ was converted to ZnO particle, surface of which was modified by TnC forming

Scheme 1 Schematic presentation of the stepwise synthesis of ZnO@*TnC* particles.

ZnO@*TnC* as crystalline material. This new material was characterized on the basis of powder-XRD, IR, SEM and EDX analysis. The Powder-X-ray diffractogram of the ZnO@*TnC* along with *TnC* and $Zn(OH)_2$ are shown in Fig. 1, which clearly shows that the diffractogram of ZnO@*TnC* is distinctly different from that of $Zn(OH)_2$ and *TnC* and there is no unreacted $Zn(OH)_2$ in the *TnC* containing new material.

The characteristic 2θ peaks for $Zn(OH)_2$ observed at 20.26°, 20.99, 25.13°, 27.29°, 27.87°, 32.94°, 39.60°, 40.86° and 42.20°, which are correspond to the orthorhombic zinc hydroxide (Fig. 1, JCPDS No: 01-089-0138)[29] are disappeared in the diffractogram of ZnO@*TnC*. The new 2θ peaks noted at 31.83°, 34.70°, 36.46°, 47.73°, 56.75°, 63.01°, 66.54°, 68.12° and 69.27° are correspond to ZnO (Fig. 1, JCPDS file no: 01-089-1397),[29] that confirmed the conversion of $Zn(OH)_2$ to ZnO. The 2θ peaks observed for *TnC* at 23.18°, 29.50, 36.10°, 39.53°, 43.28°, 47.58°, 48.61°, 57.51° and 60.79° (Fig. 1) are almost disappeared or shifted in the diffractogram observed for ZnO@*TnC*, indicating that the added *TnC* is consumed for functionalization of the surface of the ZnO particles and almost nothing is left free contaminating the functionalized composite material (ZnO@*TnC*). The IR spectra of *TnC* and that of ZnO@*TnC* are displayed in Fig. S1 (ESI),† the *TnC* exhibits IR bands at 3450, 1633, 1435 and 1076 cm^{-1}, which are due to –OH, carbonyl group, carboxyl stretching and asymmetric stretching of carboxyl group.[30] The IR spectrum of ZnO@*TnC* exhibits similar bands with slight shift in position at 3425, 1627, 1457 and 1093 cm^{-1}; with decrease in the intensity of bands at 1457 and

1093 cm^{-1} confirming functionalization of TnC over ZnO particles. The bands were shifted due to interaction of the functional groups with the ZnO particles. The IR data therefore, suggest the presence of *TnC* in the crystals of ZnO@*TnC* and probably anchoring through the surface of the particles took place through the carboxylic groups, as its band intensity and position affected significantly due to surface modification by *TnC*. The crystallite size of ZnO and ZnO@TnC was calculated following the literature procedure[31] and the results showed that the crystallite size of ZnO before and after functionalization are 236.022 and 295.021 nm, respectively, it is increased significantly confirming the functionalization. The modification of the surface of ZnO is also evident from SEM images and EDX analysis. The FE-SEM images of ZnO, before and after coating with *TnC*, and EDX analysis of the ZnO@*TnC* are shown in Fig. 2. ZnO for SEM image was prepared from $Zn(OH)_2$ by calcination in a muffle furnace by heating at 400 °C for 4 h, the XRD data of which was matched with literature values (JCPDS No: 01-089-1397).

The changes on the surface of the particles after anchoring of *TnC* is clearly seen in Fig. 2C comparing it with the surface without modification (Fig. 2A). The EDX analysis of ZnO and that of ZnO@*TnC*, shown in Fig. 2B and D, show the presence of carbon, nitrogen and high percentage of oxygen in ZnO@*TnC* compared to ZnO, confirming the presence of *TnC* in ZnO@*TnC*.

3.2. Adsorption property of ZnO@*TnC* towards metal ions and anions

Adsorption property of ZnO@*TnC* was investigated towards the metal ions Li^+, Na^+, K^+, Mg^{2+}, Mn^{2+}, Fe^{3+}, Co^{2+}, Ni^{2+}, Cu^{2+}, Hg^{2+}, Pb^{2+}, Cd^{2+} and anions AsO_2^{1-}, $Cr_2O_7^{2-}$, CN^-, F^-, PO_4^{3-} following the methods described in the Experimental section.

Bar diagram plotting the concentration of various metal ions and anions before and after adsorption is depicted in Fig. 3, which exhibited that the metal ions Fe^{3+} and Pb^{2+} and the anions PO_4^{3-} are absorbed almost the entire amount used in the experiment. Further, the Fe^{3+} adsorbed ZnO@*TnC* material
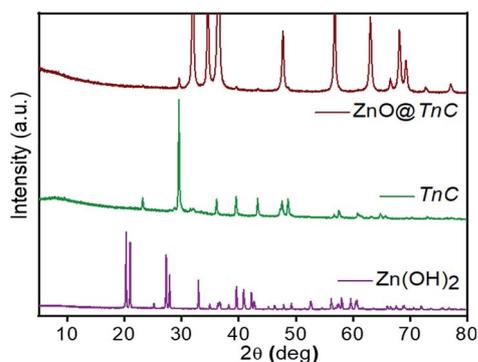

Fig. 1 Powder X-ray diffractograms of $Zn(OH)_2$ (purple color), biomass of *Tinospora cordifolia* (green color) and ZnO@*TnC* particles (brown color).
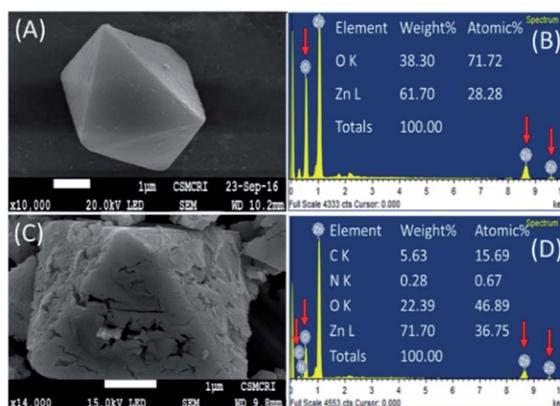

Fig. 2 SEM images of ZnO particles (A), ZnO@*TnC* particles (C) and their EDX spectra respectively (B and D). Enlarged SEM images with recording parameters is submitted as ESI (S9).†
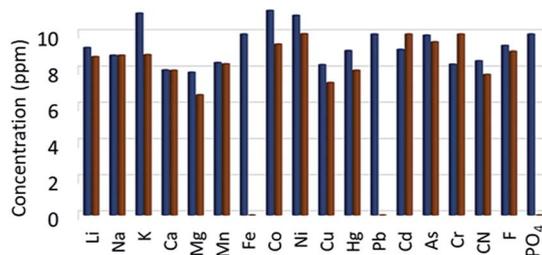
Fig. 3 Bar diagram showing concentration of different metal ions and anions before adsorption (blue bars) and after adsorption by ZnO@TnC particles (brown bars). (Oxidation state of metal ions are omitted for clarity; all metal ions are in "2+" oxidation state except iron (Fe) and Arsenic (As), which are in "3+" and chromium is in "6+" oxidation state).

(Fe–ZnO@TnC) was used for adsorption of AsO_2^{1-} from aqueous solution following the method described in the experimental section, and the concentration of AsO_2^{1-} measured before and after adsorption by IC is shown in Fig. S2 (ESI),† which clearly suggested substantial adsorption of AsO_2^{1-}. The presence of Fe^{3+}, Pb^{2+} and PO_4^{3-} in ZnO@TnC and AsO_2^{1-} in Fe–ZnO@TnC were confirmed with the aid of PXRD, IR spectroscopy and SEM microscopy, as described below.

3.3. Characterization of adsorbed ions

The adsorption of metal ions and anions on to the surface of the ZnO@TnC was confirmed on the basis of PXRD, IR and SEM analysis of the isolated ion adsorbed species of ZnO@TnC. Each of these ion adsorbed species were obtained following the procedure described in the Experimental section. The powder X-ray diffractograms of the ion adsorbed ZnO@TnC materials are shown in Fig. 4.

It may be noted that there are substantial changes in the diffractograms compared to that of ZnO@TnC after adsorption of metal ions/anions. However, the peaks observed in pure ZnO@TnC are noted as it is in all the diffractograms, the additional peaks are due to Pb^{2+}/Fe^{3+}/PO_4^{3-} adsorbed species of ZnO@TnC. In the case of AsO_2^{1-}, probably after its interaction

with Fe–ZnO@TnC, its crystallinity is lost and amorphous product is formed, as evident from the X-ray diffractogram, Fig. S3 (ESI).† The interaction of metal ion/anion with ZnO@TnC is also investigated by IR spectroscopy, shown in Fig. 5.

In Fig. 5, it may be noted that there is significant change in band position and band intensity in the region 1700–500 cm^{-1} and around 3500 cm^{-1} for all of the ion bound ZnO@TnC compared to the mother compound. Prominent changes are noted in the regions 1700–1400 cm^{-1} and 3400–3500 cm^{-1}, which are due to carbonyl/carboxylic acid groups and OH/NH groups, respectively, which suggest that the ions interacted with ZnO@TnC through the C=O/COOH and OH/NH functional groups of TnC embedded onto the surface of the ZnO particles. The IR spectrum of the AsO_2^{1-} bound Fe–ZnO@TnC, shown in Fig. S4 (ESI),† also showed significant change compared to its mother compound in the finger print region confirming the interaction of AsO_2^{1-} with Fe–ZnO@TnC. The morphology of the ion adsorbed ZnO@TnC is investigated by FE-SEM and the presence of ions ($Pb^{2+}/Fe^{3+}/PO_4^{3-}$) in it is confirmed by EDX analysis. The FE-SEM images and the EDX analysis of all the ion adsorbed ZnO@TnC are shown in Fig. 6. It may be noted that on adsorption of ion, the morphology of ZnO@TnC has changed substantially and the EDX data show the presence of respective metal ion/element (P of phosphate ion). Therefore, PXRD, IR, FE-SEM and EDX analysis have confirmed the adsorption of ions by ZnO@TnC.

3.4. Removal of metal ions and anion and their quantification

The ZnO@TnC particles were used for adsorption of Pb^{2+}, Fe^{3+} and PO_4^{3-} and Fe–ZnO@TnC was used for adsorption of AsO_2^{1-} in aqueous media at different concentration of metal ions/anions.

Details of the procedure is given in the Experimental section and the plot of amount of metal ion/anion adsorbed as a function of time at different concentrations are shown in Fig. 7. It is observed that in the case of Pb^{2+} and Fe^{3+}, saturation of
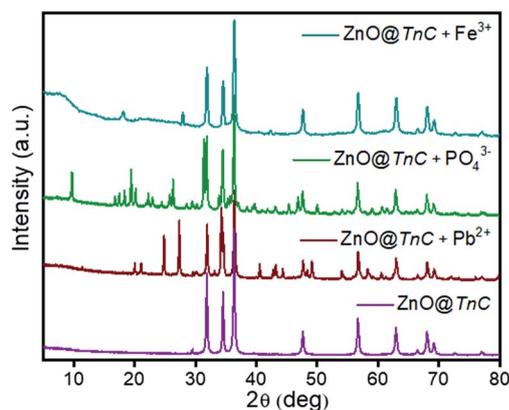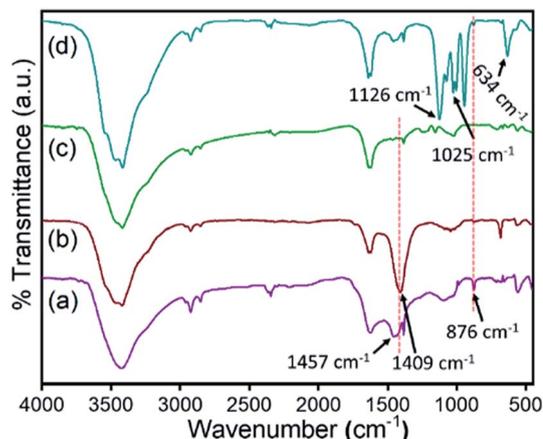

Fig. 4 XRD spectral analysis of ZnO@TnC (purple color) and that after adsorption of Pb^{2+} (brown color), PO_4^{3-} (green color) and Fe^{3+} (dark cyan color).

Fig. 5 IR spectra of the ZnO@TnC (a) and that after adsorption of Pb^{2+} (b), Fe^{3+} (c) and PO_4^{3-} (d).
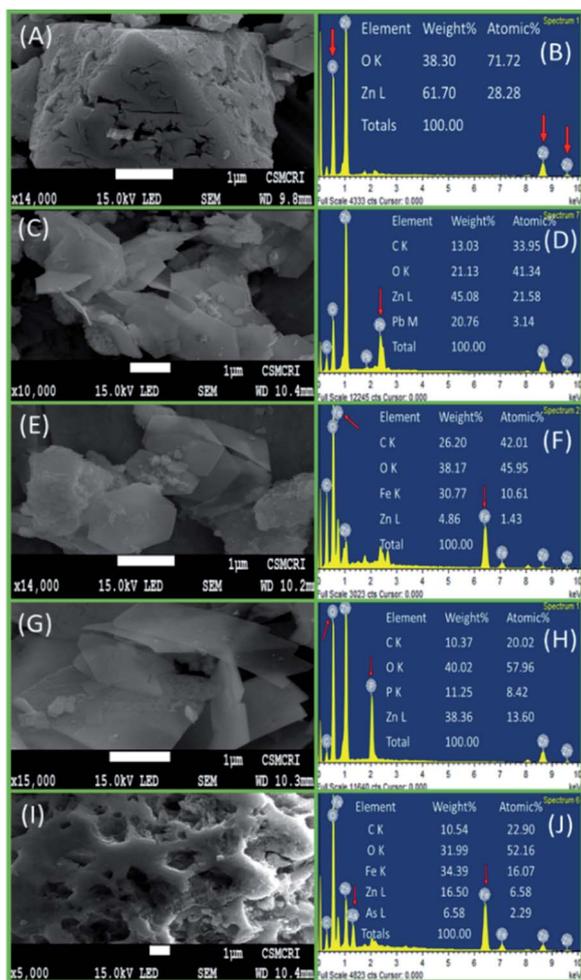
Fig. 6 SEM images along with EDX spectra of (A and B) ZnO@*TnC* particles after adsorption of (C and D) Pb^{2+}, (E and F) Fe^{3+}, (G and H) PO_4^{3-} and (I and J) AsO_2^{1-} adsorbed Fe–ZnO@*TnC*. Enlarged SEM images with recording parameters is submitted as ESI (S9).†

and Freundlich isotherm models. According to the Langmuir model, most of the adsorption occurs on the surface of the adsorbent and migration of adsorbate molecules do not occur. Mathematically, Langmuir isotherm can be expressed by the following equation.[53]

Langmuir isotherm

$$q_e = \frac{Q_m K_L C_e}{1 + K_L C_e} \quad (2)$$

where "q_e" is the quantity of the adsorbed adsorbate at the time of equilibrium, "C_e" is the concentration of adsorbate remained at the time of equilibrium, "Q_m" is the quantity of adsorbate adsorbed on the adsorbent at saturation point and "K_L" is Langmuir constant. The above Langmuir isotherm can be rewritten in the following way and the plot $1/q_e$ Vs $1/C_e$ is expected to be linear.

$$\frac{1}{q_e} = \frac{1}{Q_m} + \frac{1}{Q_m K_L} \frac{1}{C_e} \quad (3)$$

An essential characteristic of the Langmuir adsorption isotherm can be expressed by dimensionless factor, also called equilibrium parameter (R_L), which can be calculated using the following eqn (4).[54]

$$R_L = \frac{1}{1 + K_L C_0} \quad (4)$$

where K_L is the Langmuir constant and C_0 is the initial concentration of the analyte. If the R_L values is $0 < 1$ then the Langmuir adsorption is favorable and if $R_L > 1$, then the adsorption is unfavorable.

Freundlich adsorption isotherm is mainly describe multilayer adsorption in liquid to solid phase. Freundlich isotherm can be expressed in the following way.[53]
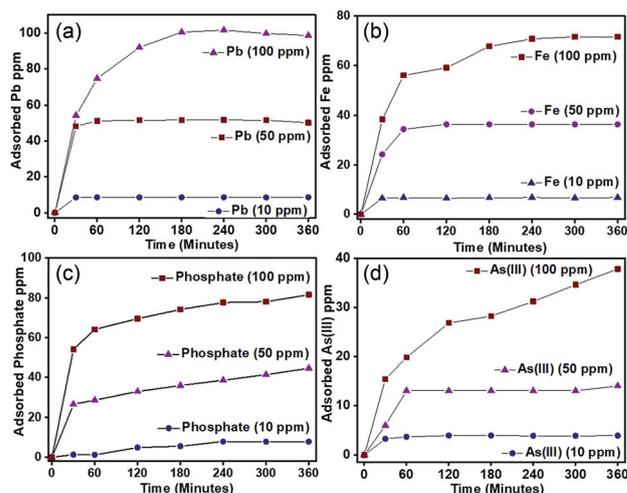
Freundlich isotherm

$$q_e = k_f C_e^{\frac{1}{n}} \quad (5)$$

adsorption is reached by 180 minutes, while in the case of PO_4^{3-} and AsO_2^{1-}, saturation was observed after 240 and 360 minutes, respectively. The adsorption capacity of Pb^{2+}, Fe^{3+}, PO_4^{3-}, calculated by using eqn (1), was found to be 506.1 mg g^{-1}, 358 mg g^{-1} and 1606 mg g^{-1}, respectively and the same for AsO_2^{1-} was to be 189 mg g^{-1}. The adsorption capacities thus obtained were compared with that of a number of recently published systems, functionalized with various materials (Table 1) and it is noted that the data obtained by the present study are comparable and in many cases better than the reported values. Apparently, the removal capacity obtained for PO_4^{3-} by present study is one of the highest among the reported values. The experimental data thus obtained was further used to determine kinetics and adsorption isotherm model.

3.5. Adsorption isotherm of ZnO@*TnC*

To evaluate the adsorption efficiency of ZnO@*TnC* towards Pb^{2+}, Fe^{3+}, PO_4^{3-} and of Fe–ZnO@*TnC* towards AsO_2^{1-}, the experimental data was fitted with classical Langmuir isotherm

Fig. 7 Kinetic study of ions (a) Pb^{2+}, (b) Fe^{3+}, (c) PO_4^{3-} and (d) AsO_2^{1-} at their initial concentration of 10, 50 and 100 ppm with time.

Table 1 Comparison of different previously reported tool and their adsorption capacity towards Pb^{2+}, Fe^{3+}, PO_4^{3-} and AsO_2^{1-} in aqueous media

Material used	Adsorption capacity (mg g^{-1})				
	Pb^{2+}	Fe^{3+}	AsO_2^{1-}	PO_4^{3-}	Ref.
Saraca indica leaf powder	1.19	—	—	—	32
Titanate/Fe_3O_4 nano	382.3	—	—	—	33
Poly(ethyleneimine) nano rod	240	—	—	—	34
Nano vaterite poly(ethyleneimine)	2762	—	—	—	35
MFe_2O_4 (M = Mn, Co)–MoS_2–carbon dot	588.2	—	—	—	36
ZnO/MMT nanocomposite	88.50	—	—	—	37
Fly ash	—	—	—	42.5	38
Magnetic cellulose	—	—	—	22.2	39
Biomass based $Zr(OH)_4$	—	—	—	31.9	40
Biochar (Mg-enriched tomato tissues)	—	—	—	>100	41
Mesoporous silica	—	—	—	43.3	42
Ferric sludge	—	—	—	30	43
Natural zeolite	—	1.15	—	—	44
Natural smectite clay	—	12.8	—	—	45
Vegetable biomass	—	3.5	—	—	46
Activated carbon	—	3.60	—	—	47
Nano zero-valent iron	—	—	3.5	—	48
Fe/Cu nanoparticles	—	—	19.6	—	49
Magnetic Fe_3O_4 nano	—	—	19.6	—	50
$(Sn_{0.95}Fe_{0.05}O_{2-\delta})$@GO	—	—	105	—	51
Nano cellulose	—	—	51	—	52
ZnO@*TnC* particles	506.1	358	189	1606	This study

where "q_e" and "C_e" terms are same as described in Langmuir equation, "K_f" is the Freundlich constant and "n" is the Freundlich exponent which is related to the heterogeneity of the surface of adsorbent. The simplified form of the above equation can be rewritten as below.

$$\log q_e = \log K_f + \frac{1}{n} \log C_e \qquad (6)$$

The experimental adsorption data were fitted in the eqn (3) and (5) and the plot of Langmuir and Freundlich adsorption isotherms for metal ions and anion are shown in Fig. 8 and S5
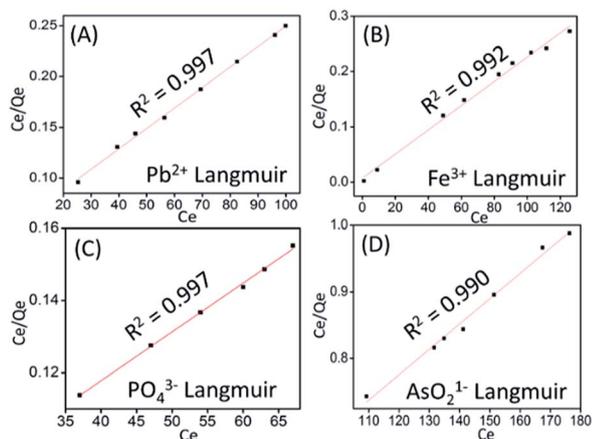
(ESI),† respectively. The dimensionless factor (R_L) is calculated using the eqn (4) and all the calculated parameters and the correlation coefficient (R^2) values obtained from the plot are summarized in Table 2. The R_L values obtained is 0 < 1, which suggests that the Langmuir adsorption is favorable. Schematic presentation of monolayer adsorption of Pb^{2+} and Fe^{3+} is shown in the Scheme 2a. Higher value of Freundlich adsorption exponent "n", which is equal to or greater than 1, suggests that adsorption is favorable on surface of the particles.[55] It may be noted that the adsorption isotherm study with different ions were carried out with the solutions of concentrations 10, 50 and 100 ppm and the adsorption capacity thus obtained has given in Table 1. However, it was noted that in case of Pb^{2+} and PO_4^{3-}, the saturation point was not achieved with 100 ppm solution, therefore to examine the maximum adsorption capacity, experiment was repeated with 1000 ppm solution for these two ions and the data obtained is presented in Table 2. To maintain

Fig. 8 Plot of C_e/Q_e Vs C_e representing linearized form of Langmuir adsorption isotherm of (A) Pb^{2+} (B), Fe^{3+} (C) PO_4^{3-} and (D) AsO_2^{1-}.

Table 2 Langmuir and Freundlich adsorption isotherm model parameters for Pb^{2+}, Fe^{3+}, PO_4^{3-} and AsO_2^{1-} adsorption by ZnO@*TnC* particles

Metal ions	Langmuir adsorption isotherm				Freundlich adsorption isotherm		
	K_L	Q_m	R_L	R^2	K_F	n	R^2
Pb^{2+}	0.042	497.51	0.15	0.997	3.68	2.72	0.924
Fe^{3+}	0.302	456.62	0.02	0.992	4.99	6.10	0.906
PO_4^{3-}	0.021	740.74	0.29	0.997	1.60	0.90	0.988
AsO_2^{1-}	0.011	262.46	0.31	0.990	0.06	0.33	0.977
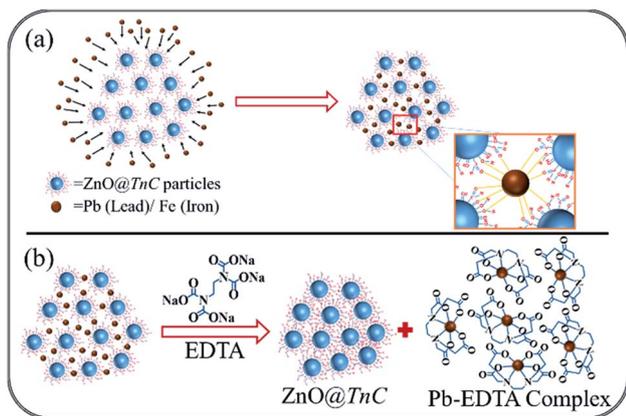
Scheme 2 Schematic presentation of (a) monolayer adsorption of Pb^{2+} and Fe^{3+} by ZnO@TnC particles and (b) regeneration of ZnO@TnC particles by desorption of Pb^{2+} after treatment with EDTA.

uniformity, the adsorption capacity data for all the ions with 100 ppm solution has given in Table 1.

3.6. Adsorption kinetics

For insight of mechanistic aspects, kinetics of the adsorption process was also carried out, experimental procedure for which is described in the Experimental section. For this purpose, two semi empirical kinetic models (i) pseudo-first-order and (ii) pseudo-second-order, which are based on adsorption equilibrium capacity, is used.[56] The equation for pseudo first order reaction is shown below.

$$\frac{dQ_t}{d_t} = k_1(Q_e - Q_t) \tag{7}$$

where Q_e and Q_t are the adsorbed amounts of metal ions/anions at equilibrium and time 't', respectively; k_1 is the pseudo-first-order kinetic constant, expressed in inverse minutes. Equation integration and rearrangement yields the linear form as shown below.

$$\ln(Q_s - Q_t) = \ln Q_e - k_1 t \tag{8}$$

The equation for pseudo second order reaction can be expressed mathematically as shown below.

$$\frac{dQ_t}{d_t} = k_2(Q_e - Q_t)^2 \tag{9}$$

where Q_e and Q_t are same as in eqn (6); k_2 (g (mol min)$^{-1}$) is the pseudo-second-order rate constant. The differential equation is usually integrated and transformed in its linear form as shown below.

$$\frac{t}{Q_t} = \frac{1}{k_2 Q_e^2} + \frac{t}{Q_e} \tag{10}$$

Experimental data obtained from the kinetic study following the procedure described in the Experimental section is fitted in eqn (7) and (9) and the plot obtained for pseudo-second-order

and pseudo-first-order are shown in Fig. 9 and S6 (ESI),† respectively.

The values of correlation co-efficient (R^2) obtained for all metal ions and anions at different concentrations using both the equations are summarized in Table S1.† The R^2 values suggests that the experimental data are better fitted with the pseudo-second-order equation. The rate constant and other parameters are therefore, calculated using the pseudo-second-order equation and the data are summarized in Table 3. It can be observed from Table 3 that, in case of Pb^{2+} and Fe^{3+}, initial adsorption (h) increases with increase in metal ion concentration from 10 to 50 ppm and then decreases it at 100 ppm, which indicated the saturation of ZnO@TnC with metal ions. However, in case of PO_4^{3-} and AsO_2^{1-}, "h" increases with increase in the concentration of ions from 10 to 100 ppm, which indicated availability of more binding site on the particles.[57] Rate constant of pseudo-second-order kinetic "k_2" decreases with increase in initial concentration of ions. In all cases, the amount of metal ions adsorbed increases with increase in their initial concentration. Adsorption capacity of Pb^{2+}, Fe^{3+} and PO_4^{3-} was found to be 506.1 mg g^{-1}, 358 mg g^{-1} and 1606 mg g^{-1}, respectively by ZnO@TnC and of AsO_2^{1-} to be 189 mg g^{-1} by Fe–ZnO@TnC.

3.7. Adsorption with variation in pH

Adsorption of all ions were conducted in the pH range 2 to 12 following the procedure described in the Experimental section. For $PbCl_2$, however the study was conducted up to pH 9 due to insufficient solubility of $PbCl_2$ at higher pH. The bar diagram showing the amount of ions adsorbed at different pH is displayed in Fig. S7 (ESI),† which shows that except PO_4^{3-}, adsorption of all other ions are independent of pH. In case of PO_4^{3-}, its adsorption was observed to be higher at acidic pH and lower at higher (basic) pH. This is probably due to the fact that PO_4^{3-} binds with ZnO@TnC through H-bonding and at higher pH the binding sites get deprotonated.
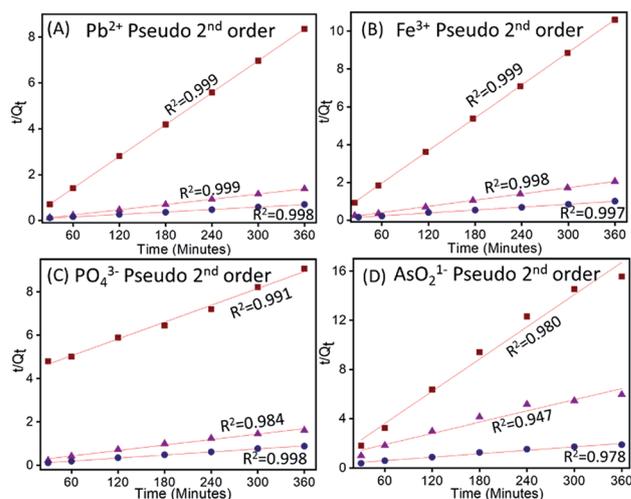

Fig. 9 Plot of pseudo-second-order kinetic study of (A) Pb^{2+} (B) Fe^{3+} (C) PO_4^{3-} and (D) AsO_2^{1-} adsorption by ZnO@TnC.

Table 3 Pseudo first and second order kinetic model parameters for Pb^{2+}, Fe^{3+}, PO_4^{3-} and AsO_2^{1-} adsorption by ZnO@TnC

| Initial conc. (PPM)	k_2 (g mg^{-1} min^{-1})	h (mg g^{-1} min^{-1})	Q_e (mg g^{-1}) practical	Q_e (mg g^{-1}) calculated
Pb^{2+}				
10	3.68×10^{-2}	68.57	43.11	43.15
50	2.35×10^{-3}	160.72	260.10	261.09
100	6.69×10^{-5}	20.89	512.25	558.65
Fe^{3+}				
10	1.17×10^{-2}	13.75	33.97	34.19
50	9.09×10^{-4}	29.32	175.25	179.53
100	8.95×10^{-5}	13.65	358.35	390.62
PO_4^{3-}				
10	1.23×10^{-4}	0.23	39.68	38.49
50	1.12×10^{-4}	6.33	222.90	237.52
100	1.10×10^{-4}	20.03	408.00	425.53
AsO_2^{1-}				
10	3.67×10^{-4}	0.19	23.15	22.90
50	8.73×10^{-5}	0.38	60.50	66.26
100	2.45×10^{-5}	1.13	189.00	214.59

3.8. Recovery of ZnO@TnC for reuse

The possibility to recover the ZnO@TnC by desorption of adsorbed metal ion to reuse it for further adsorption study is investigated. Detail experimental procedure has given in the Experimental section. For desorption of Pb^{2+}, a strong chelating agent called ethylenediaminetetraacetate (EDTA) was added into Pb^{2+}–ZnO@TnC, which resulted in formation of water soluble Pb^{2+}–EDTA complex, the suspended ZnO@TnC was then separated by centrifugation and after washing the solid by water it is reused for adsorption of Pb^{2+} up to 3 consecutive cycles as shown in the Fig. S8A (ESI).† The schematic presentation of desorption of Pb^{2+} and formation of Pb^{2+}–EDTA complex is depicted in Scheme 2b. As mentioned earlier, PO_4^{3-} at higher pH does not interact with ZnO@TnC due to

deprotonation of its binding sites, therefore ZnO@TnC after adsorption of PO_4^{3-} was treated with NaOH solution, which induced deprotonation of the functional group (Scheme 3), resulting in the release of PO_4^{3-} in the solution. After NaOH treatment, it was neutralized with HCl solution and then reused for further adsorption of PO_4^{3-}.

ZnO@TnC was reused for PO_4^{3-} adsorption up to 3 consecutive cycle as shown in Fig. S8B (ESI).† The chelating agent EDTA, however was not effective for releasing Fe^{3+} from Fe–ZnO@TnC. However, Fe–ZnO@TnC was used further for the adsorption of AsO_2^{1-} in aqueous media. Attempt has been made for regeneration of ZnO@TnC from AsO_2^{1-} adsorbed Fe–ZnO@TnC materials by desorption of AsO_2^{1-} and Fe^{3+} by variation of pH and treatment with EDTA but it was not successful.

4. Conclusions

The present study demonstrated an easy and simple method for the preparation of a biomass grafted ZnO microcrystalline material as an adsorbent for selected metal ions and anions. The biomass powder was prepared from *Tinospora cordifolia* and it was anchored on to the surface of the ZnO particles by calcination of $Zn(OH)_2$ in presence of the biomass. The surface functionalized ZnO particles (ZnO@TnC) adsorbed Pb^{2+}, Fe^{3+} and PO_4^{3-} effectively out of a large number of metal ions and anions examined and the Fe^{3+} adsorbed ZnO@TnC material further adsorbed AsO_2^{1-}. The amount of PO_4^{3-} absorbed, 1606 mg g^{-1}, is the highest so far reported to the best of our knowledge. The amount of Pb^{2+} (506.1 mg g^{-1}) and Fe^{3+} (358 mg) adsorbed is also very high and are comparable to some of the best systems reported recent time. For Pb^{2+} and PO_4^{3-}, the reusability of ZnO@TnC is demonstrated by desorption of the metal ion and anion for three cycle without deactivation. For Fe^{3+}, the metal ion adsorbed material was further used to
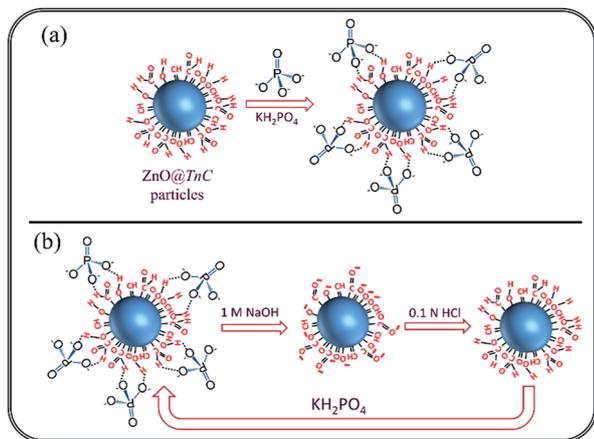
Scheme 3 Schematic presentation of (a) adsorption of PO_4^{3-} by ZnO@TnC and (b) regeneration of ZnO@TnC by desorption of PO_4^{3-} after treatment with 1 mol L^{-1} naOH solution.

adsorb AsO_2^{1-}. The experimental adsorption data fitted excellently with the Langmuir adsorption isotherm model and the adsorption kinetic data follow the pseudo-second-order equation. All of the calculated parameters are reported and the possible mechanism of adsorption is presented. The material developed following a simple method using low cost starting materials and is very useful for removal of Pb^{2+}, Fe^{3+}, PO_4^{3-} and AsO_2^{1-} from the waste water and industrial effluents.

Conflicts of interest

There are no conflicts to declare.

Acknowledgements

Notes and references

1 T. Tong and M. Elimelech, The Global Rise of Zero Liquid Discharge for Wastewater Management: Drivers, Technologies, and Future Directions, *Environ. Sci. Technol.*, 2016, **50**(13), 6846–6855.

2 A. B. Boehm, K. E. Graham and W. C. Jennings, Can We Swim Yet? Systematic Review, Meta-Analysis, and Risk Assessment of Aging Sewage in Surface Waters, *Environ. Sci. Technol.*, 2018, **52**(17), 9634–9645.

3 N. Saha, M. S. Rahman, M. B. Ahmed, J. L. Zhou, H. H. Ngo and W. Guo, Industrial Metal Pollution in Water and Probabilistic Assessment of Human Health Risk, *J. Environ. Manage.*, 2017, **185**, 70–78.

4 B. Moss, Water Pollution by Agriculture, *Philos. Trans. R. Soc., B*, 2008, **363**(1491), 659–666.

5 F. M. Rebelo and E. D. Caldas, Arsenic, Lead, Mercury and Cadmium: Toxicity, Levels in Breast Milk and the Risks for Breastfed Infants, *Environ. Res.*, 2016, **151**, 671–688.

6 G. Flora, D. Gupta and A. Tiwari, Toxicity of Lead: A Review with Recent Updates, *Interdiscip. Toxicol.*, 2012, **5**(2), 47–58.

7 B. E. Hettick, J. E. Canas-Carrell, A. D. French and D. M. Klein, Arsenic: A Review of the Element's Toxicity, Plant Interactions, and Potential Methods of Remediation, *J. Agric. Food Chem.*, 2015, **63**(32), 7097–7107.

8 E. Topuz, O. V. Erkan and I. Talinli, Waste Management Strategies for Cleaner Recycling of Spent Batteries: Lead Recovery and Brick Production from Slag, *Int. J. Environ. Sci. Technol.*, 2019, DOI: 10.1007/s13762-019-02308-4.

9 B. Ericson, P. Landrigan, M. P. Taylor, J. Frostad, J. Caravanos, J. Keith and R. Fuller, The Global Burden of Lead Toxicity Attributable to Informal Used Lead-Acid Battery Sites, *Ann. Glob. Health.*, 2016, **82**(5), 686–699.

10 T. L. Pan, P. W. Wang, S. A. Al-Suwayeh, C. C. Chen and J. Y. Fang, Skin Toxicology of Lead Species Evaluated by Their Permeability and Proteomic Profiles: A Comparison of Organic and Inorganic Lead, *Toxicol. Lett.*, 2010, **197**(1), 19–28.

11 M. Jaishankar, T. Tseten, N. Anbalagan, B. B. Mathew and K. N. Beeregowda, Toxicity, Mechanism and Health Effects of Some Heavy Metals, *Interdiscip. Toxicol.*, 2014, **7**(2), 60–72.

12 W. Q. Chen, Y. L. Shi, S. L. Wu and Y. G. Zhu, Anthropogenic Arsenic Cycles: A Research Framework and Features, *J. Cleaner Prod.*, 2016, **139**, 328–336.

13 H. T. Hanh, J. Y. Kim, S. Bang and K. W. Kim, Sources and Fate of As in the Environment, *Geosyst. Eng.*, 2010, **13**(1), 35–42.

14 T. S. Y. Choong, T. G. Chuah, Y. Robiah, F. L. Gregory Koay and I. Azni, Arsenic Toxicity, Health Hazards and Removal Techniques from Water: An Overview, *Desalination*, 2007, **217**(1–3), 139–166.

15 G. Vyas, A. Kumar, M. Bhatt, S. Bhatt and P. Paul, New Route for Synthesis of Fluorescent SnO_2 Nanoparticles for Selective Sensing of Fe(III) in Aqueous Media, *J. Nanosci. Nanotechnol.*, 2018, **18**, 3954–3959.

16 V. Kumar, P. K. Bharti, M. Talwar, A. K. Tyagi and P. Kumar, Studies on High Iron Content in Water Resources of Moradabad District (UP), India, *Water Science*, 2017, **31**(1), 44–51.

17 B. Kestenbaum, J. N. Sampson, K. D. Rudser, D. J. Patterson, S. L. Seliger, B. Young, D. J. Sherrard and D. L. Andress, Serum Phosphate Levels and Mortality Risk among People with Chronic Kidney Disease, *J. Am. Soc. Nephrol.*, 2005, **16**, 520–528.

18 S. M. Harris, J. T. Nguyen, S. L. Pailloux, J. P. Mansergh, M. J. Dresel, T. B. Swanholm, T. Gao and V. C. Pierre, Gadolinium Complex for the Catch and Release of Phosphate from Water, *Environ. Sci. Technol.*, 2017, **51**(8), 4549–4558.

19 S. K. Gunatilake, Methods of Removing Heavy Metals From Industrial Wastewater, *J. Multidiscip. Eng. Sci. Stud.*, 2015, **1**(1), 13–18.

20 C. A. Basha, N. S. Bhadrinarayana, N. Anantharaman and K. M. Meera Sheriffa Begum, Heavy Metal Removal from Copper Smelting Effluent Using Electrochemical Cylindrical Flow Reactor, *J. Hazard. Mater.*, 2008, **152**(1), 71–78.

21 A. Dabrowski, Z. Hubicki, P. Podkoscielny and E. Robens, Selective Removal of the Heavy Metal Ions from Waters and Industrial Wastewaters by Ion-Exchange Method, *Chemosphere*, 2004, **56**(2), 91–106.

22 V. K. Gupta, I. Ali, T. A. Saleh, A. Nayak and S. Agarwal, Chemical Treatment Technologies for Waste-Water Recycling – An Overview, *RSC Adv.*, 2012, **2**(16), 6380–6388.

23 Y. R. Zhao, Z. R. Zhang, C. Yang, H. L. Fan, J. Wang, Z. Tian and H. Y. Zhang, Critical Role of Water on the Surface of ZnO in H_2S Removal at Room Temperature, *Ind. Eng. Chem. Res.*, 2018, **57**, 15366–15374.

24 S. Alhan, M. Nehra, N. Dilbaghi, N. K. Singhal, K. H. Kim and S. Kumar, Potential use of ZnO@activated carbon nanocomposites for the adsorptive removal of Cd^{2+} ions in aqueous solutions, *Environ. Res.*, 2019, **173**, 411–418.

25 I. Ghiloufi, J. El Ghoul, A. Modwi and L. El Mir, Ga-Doped ZnO for Adsorption of Heavy Metals from Aqueous Solution, *Mater. Sci. Semicond. Process.*, 2016, **42**(3), 102–106.

26 A. S. Ibupoto, U. A. Qureshi, M. Arain, F. Ahmed, Z. Khatri, R. Z. Brohi, I. S. Kim and Z. I. Ahmad, ZnO/Carbon nanofibers for efficient adsorption of lead from aqueous solutions, *Environ. Technol.*, 2019, DOI: 10.1080/0959330.2019.1580774.

27 K. Sao, M. Pandey, P. K. Pandey and F. Khan, Highly Efficient Biosorptive Removal of Lead from Industrial Effluent, *Environ. Sci. Pollut. Res.*, 2017, **24**(22), 18410–18420.

28 Z. Aly, A. Graulet, N. Scales and T. Hanley, Removal of Aluminium from Aqueous Solutions Using PAN-Based Adsorbents: Characterisation, Kinetics, Equilibrium and Thermodynamic Studies, *Environ. Sci. Pollut. Res.*, 2014, **21**(5), 3972–3986.

29 M. Podlogar, A. Recnik, G. Yilmazoglu, I. O. Ozer, M. Mazaj, E. Suvaci and S. Bernik, The Role of Hydrothermal Pathways in the Evolution of the Morphology of ZnO Crystals, *Ceram. Int.*, 2016, **42**(14), 15358–15366.

30 K. Sao, F. Khan, P. K. Pandey and M. Pandey, Equilibrium Isotherm Study for Removal of Mn(II) from Aqueous Solutions by Using Novel Bioadsorbent *Tinospora cordifolia*, *J. Adv. Res.*, 2016, **6**(4), 1–11.

31 V. J. Inglezakis, S. G. Poulopoulos and H. Kazemian, Insights into the S-shaped sorption isotherms and their dimensionless forms, *Microporous Mesoporous Mater.*, 2018, **272**, 166–176.

32 P. Goyal, P. Sharma, S. Srivastava and M. M. Srivastava, Saraca Indica Leaf Powder for Decontamination of Pb: Removal, Recovery, Adsorbent Characterization and Equilibrium Modeling, *Int. J. Environ. Sci. Technol.*, 2008, **5**(1), 27–34.

33 F. Liu, Y. Jin, H. Liao, L. Cai, M. Tong and Y. Hou, Facile self-assembly synthesis of titanate/Fe_3O_4 nanocomposites for the efficient removal of Pb^{2+} from aqueous systems, *J. Mater. Chem. A*, 2013, **1**, 805–813.

34 A. M. Lopez-Marzo, J. Pons and A. Merkoci, Multifunctional system based on hybrid nanostructured rod formation, for sensoremoval applications of Pb^{2+} as a model toxic metal, *J. Mater. Chem. A*, 2013, **1**, 13532–13541.

35 A. M. Lopez-Marzo, J. Pons and A. Merkoci, Extremely fast and high Pb^{2+} removal capacity using a nanostructured hybrid material, *J. Mater. Chem. A*, 2014, **2**, 8766–8772.

36 J. Wang, W. Zhang, X. Yue, Q. Yang, F. Liu, Y. Wang, D. Zhang, Z. Li and J. Wang, One-pot synthesis of multifunctional magnetic ferrite–MoS_2–carbon dot nanohybrid adsorbent for efficient Pb(II) removal, *J. Mater. Chem. A*, 2016, **4**, 3893–3900.

37 H. A. Sani, M. B. Ahmad, M. Z. Hussein, N. A. Ibrahim, A. Musa and T. A. Saleh, Nanocomposite of ZnO with Montmorillonite for Removal of Lead and Copper Ions from Aqueous Solutions, *Process Saf. Environ. Prot.*, 2017, **109**, 97–105.

38 J. Chen, H. Kong, D. Wu, X. Chen, D. Zhang and Z. Sun, Phosphate Immobilization from Aqueous Solution by Fly Ashes in Relation to Their Composition, *J. Hazard. Mater.*, 2007, **139**, 293–300.

39 X. Lei, X. Dai, S. Long, N. Cai, Z. Ma and X. Luo, Facile Design of Green Engineered Cellulose/Metal Hybrid Macrogels for efficient Trace Phosphate Removal, *Ind. Eng. Chem. Res.*, 2017, **56**, 7525–7533.

40 H. Qiu, C. Liang, X. Zhang, M. Chen, Y. Zhao, T. Tao, Z. Xu and G. Liu, Fabrication of a Biomass-Based Hydrous Zirconium Oxide Nanocomposite for Preferable Phosphate Removal and Recovery, *ACS Appl. Mater. Interfaces*, 2015, **7**, 20835–20844.

41 Y. Yao, B. Gao, J. Chen and L. Yang, Engineered Biochar Reclaiming Phosphate from Aqueous Solutions: Mechanisms and Potential Application as a Slow-Release Fertilizer, *Environ. Sci. Technol.*, 2013, **47**, 8700–8708.

42 W. Chouyyok, R. J. Wiacek, K. Pattamakomsan, T. Sangvanich, R. M. Grudzien and G. E. Fryxell, Phosphate Removal by Anion Binding on Functionalized Nanoporous Sorbents, *Environ. Sci. Technol.*, 2010, **44**, 3073–3078.

43 X. Song, Y. Pan, Q. Wu, Z. Cheng and W. Ma, Phosphate Removal from Aqueous Solutions by Adsorption Using Ferric Sludge, *Desalination*, 2011, **280**, 384–390.

44 M. A. Shavandi, Z. Haddadian, M. H. S. Ismail, N. Abdullah and Z. Z. Abidin, Journal of the Taiwan Institute of Chemical Engineers Removal of Fe(III), Mn(II) and Zn(II) from Palm Oil Mill Effluent (POME) by Natural Zeolite, *J. Taiwan Inst. Chem. Eng.*, 2012, **43**, 750–759.

45 L. Khalfa, M. L. Cervera, S. Souissi-najjar and M. Bagane, Removal of Fe(III) from synthetic wastewater into raw and modified clay: Experiments and models fitting, *Sep. Sci. Technol.*, 2017, 1–11.

46 R. Bun-ei, N. Kawasaki, F. Ogata, T. Nakamura, K. Aochi and S. Tanada, Removal of Lead and Iron Ions by Vegetable Biomass in Drinking water, *J. Oleo Sci.*, 2006, **55**, 423–427.

47 A. B. Jusoh, W. H. Cheng, W. M. Low, A. Noraaini and M. J. M. Mohd Noor, Study on the Removal of Iron and Manganese in Groundwater by Granular Activated Carbon, *Desalination*, 2005, **182**, 347–353.

48 S. R. Kanel, B. Manning, L. Charlet and H. Choi, Removal of Arsenic(III) from Groundwater by Nanoscale Zero-Valent Iron, *Environ. Sci. Technol.*, 2005, **39**(5), 1291–1298.

49 Y. Babaee, C. N. Mulligan and S. Rahaman, Removal of Arsenic(III) and Arsenic(V) from Aqueous Solutions through Adsorption by Fe/Cu Nanoparticles, *J. Chem. Technol. Biotechnol.*, 2018, **93**, 63–71.

50 R. M. Dhoble, P. R. Maddigapu, A. G. Bhole and S. Rayalu, Development of Bark-Based Magnetic Iron Oxide Particle (BMIOP), a Bio-Adsorbent for Removal of Arsenic(III) from Water, *Environ. Sci. Pollut. Res.*, 2018, **25**, 19657–19674.

51 M. Sharma, S. Ramakrishnan, S. Remanan, G. Madras and S. Bose, Nano-Structures & Nano-Objects Nano Tin Ferrous Oxide Decorated Graphene Oxide Sheets for Efficient

Arsenic(III) Removal, *Nano-Struct. Nano-Objects*, 2018, **13**, 82–92.

52 S. Hokkanen, B. Doshi, V. Srivastava, L. Puro and R. Koivula, Arsenic(III) Removal from Water by Hydroxyapatite-Bentonite Clay-Nanocrystalline Cellulose, *Environ. Prog. Sustainable Energy*, 2019, DOI: 10.1002/ep.13147.

53 B. E. Reed and M. R. Matsumoto, Modeling Cadmium Adsorption by Activated Carbon Using the Langmuir and Freundlich Isotherm Expressions, *Sep. Sci. Technol.*, 1993, **28**, 2179–2195.

54 N. Ayawei, A. N. Ebelegi and D. Wankasi, Modelling and Interpretation of Adsorption Isotherms, *J. Chem.*, 2017, **2017**, 3039817–3039827.

55 A. M. Aljeboree, A. N. Alshirifi and A. F. Alkaim, Kinetics and Equilibrium Study for the Adsorption of Textile Dyes on Coconut Shell Activated Carbon, *Arabian J. Chem.*, 2017, **10**, S3381–S3393.

56 J. P. Simonin, On the Comparison of Pseudo-First Order and Pseudo-Second Order Rate Laws in the Modeling of Adsorption Kinetics, *Chem. Eng. J.*, 2016, **300**, 254–263.

57 Z. Aly and V. Luca, Uranium Extraction from Aqueous Solution Using Dried and Pyrolyzed Tea and Coffee Wastes, *J. Radioanal. Nucl. Chem.*, 2013, **295**(2), 889–900.